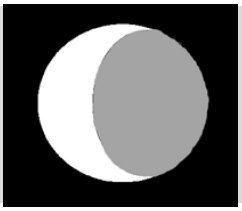

Feature Story: Concentric Lunar Craters

By Howard Eskildsen,
howardeskildsen@msn.com

Online Readers

Left-click your mouse on the e-mail address in blue text to contact the author of this article, and selected references also in blue text at the end of this paper for more information there.

This paper by ALPO member and astrophotographer Howard Eskidsen is only one of many that were presented at ALCon 2013, held in Atlanta, Georgia.

Abstract

Fifty-five concentric caters were identified and measured for diameter, depth, toroid crest diameter, coordinates, and depth/diameter (d/D) ratios were calculated using Lunar Reconnaissance Orbiter data. Crater coordinates were reproducible to within 0.02°. Outer rim diameters (D) ranged from 2.3km to 24.2 km with the mean 8.2 km with error of ± 0.2 km. Inner toroid rim diameters (T) averaged 4.3 km, and calculated toroid to diameter ratios (T/D ratio) averaged 0.51. The d/D ratios for the concentric craters averaged 0.065, much shallower than the T/D ratio of 0.20 that is typical for non-concentric craters. Mean crater rim elevations were below the mean lunar radius of 1737.4 km with the mean 1.5 km lower than the mean lunar radius.

Table 1: Eastern Hemisphere Diameter Data

	Concentric Craters Study Data								
			LROC	Mean	Geodetic		Geodetic		Mean
		Wood	QuickMap	Crater	Crater Diameter		Toroid Dameter		Toroid
	Crater	Coordinates	Coordinates	Diameter	N-S km	W-E km	N-S km	W-E km	Diameter
1	Archytas G	0.4E 55.8N	0.53E 55.74N	7.0	6.98	7.05	4.33	4.57	4.5
2	Archytas G-b		0.48E 55.56N	4.3	4.12	4.56	2.11	2.30	2.2
3	Reaumur B CC	1.3E 4.5S	1.24E 4.52S	4.4	4.14	4.67	2.76	2.87	2.8
4	Egede G	6.8E 51.9N	6.93 E 52.00N	7.3	7.25	7.26	5.34	5.32	5.3
5	Pontanus E	13.3E 25.2S	13.25E 25.22S	12.5	12.4	12.60	7.68	8.65	8.2
6	Torricelli R CC	26.6E 6.4S	26.64E 6.38S	3.8	3.80	3.82	1.18	1.27	1.2
7	Beaumont P CC	29.6E 19.1S	29.63 E 19.14S	11.7	12	11.30	5.62	5.19	5.4
8	Fracastorius E		31.02 E 20.23S	11.9	11.23	12.63	4.18	4.67	4.4
9	Crozier H	49.4E 14.1S	49.38E 14.01S	10.7	11.13	10.23	5.70	4.34	5.0
10	Endymion SW CC	50.6E 51.7N	51.06E 51.68N	6.8	6.74	6.84	2.93	2.62	2.8
11	Apollonius N	64.0E 4.7N	63.76E 4.74N	10.5	10.63	10.33	5.78	5.32	5.6
12	Legendre CC	68.2E 27.5S	68.14E 27.81S	4.4	4.55	4.22	1.62	1.52	1.6
13	Dubyago CC	69.0E 3.7N	68.61E 3.67N	5.9	5.99	5.88	2.83	2.62	2.7
14	Schubert N CC	74.0E 2.0N	73.61E 1.33N	10.2	10.11	10.24	5.59	5.44	5.5
15	Humboldt CC	83.2E 26.5S	83.36E 26.55S	8.5	8.44	8.49	3.90	3.82	3.9
16	Hamilton CC	84.7E 44.2S	84.73E 44.39S	11.6	11.4	11.70	5.57	6.19	5.9
17	Jeans CC	94.4E 53.1S	94.61E 53.13S	24.2	23.03	25.30	15.51	16.98	16.2
18	Chamberlin CC	102.5E 58.8S	102.59E 58.67S	8.3	8.16	8.53	5.88	6.64	6.3
19	Pasteur CC	104.9E 11.8S	105.15E 11.96S	6.4	6.09	6.76	3.21	3.82	3.5
20	Jules Verne CC		143.76E 37.23S	5.6	5.60	5.61	2.97	3.03	3.0
21	Jules Verne CC SE	144.1E 37.5S	144.33E 37.40S	7.1	7.29	6.95	3.61	3.78	3.7
22	Geiger CC	159.0E 16.2S	159.01 E 16.11S	6.5	6.48	6.51	2.69	2.64	2.7
23	Vertregt K CC	172.6E 20.6S	172.69E 20.50S	9.2	9.07	9.38	4.83	5.86	5.3

Table 1A: Eastern Hemisphere Elevation/Depth Data

	Concentric Craters Study Data									
			LROC					Mean Rim	Central	Mean
		Wood	QuickMap	Geodetic Crater Rim Elevation				Elevation	Elevation	Crater
	Crater	Coordinates	Coordinates	North (m)	South (m)	West (m)	East (m)	(meters)	(meters)	Depth (km)
1	Archytas G	0.4E 55.8N	0.53E 55.74N	-2680	-2490	-2690	-2440	-2575	-3010	0.435
2	Archytas G-b		0.48E 55.56N	-2650	-2680	-2066	-2550	-2486.5	-2790	0.304
3	Reaumur B CC	1.3E 4.5S	1.24E 4.52S	430	560	640	495	531.25	270	0.261
4	Egede G	6.8E 51.9N	6.93 E 52.00N	-2510	-2630	-2500	-2640	-2570	-3130	0.560
5	Pontanus E	13.3E 25.2S	13.25E 25.22S	490	640	590	510	557.5	-290	0.848
6	Torricelli R CC	26.6E 6.4S	26.64E 6.38S	-2140	-2380	-2420	-2240	-2295	-2500	0.205
7	Beaumont P CC	29.6E 19.1S	29.63 E 19.14S	-1570	-1920	-1500	-1920	-1727.5	-2250	0.523
8	Fracastorius E		31.02 E 20.23S	-1760	-900	-1500	-1060	-1305	-2200	0.895
9	Crozier H	49.4E 14.1S	49.38E 14.01S	1000	190	410	910	627.5	-380	1.008
10	Endymion SW CC	50.6E 51.7N	51.06E 51.68N	-1450	-1560	-1570	-1570	-1538	-1780	0.243
11	Apollonius N	64.0E 4.7N	63.76E 4.74N	-110	800	380	430	375	-920	1.295
12	Legendre CC	68.2E 27.5S	68.14E 27.81S	-610	-625	-720	-670	-656.25	-900	0.244
13	Dubyago CC	69.0E 3.7N	68.61E 3.67N	-920	-810	-860	-945	-883.75	-1090	0.206
14	Schubert N CC	74.0E 2.0N	73.61E 1.33N	-1230	-1410	-1680	-1430	-1437.5	-1910	0.473
15	Humboldt CC	83.2E 26.5S	83.36E 26.55S	-3500	-3490	-3410	-3500	-3475	-4380	0.905
16	Hamilton CC	84.7E 44.2S	84.73E 44.39S	-1170	-900	-1020	-1030	-1030	-1680	0.650
17	Jeans CC	94.4E 53.1S	94.61E 53.13S	190	50	-320	-380	-115	-1000	0.885
18	Chamberlin CC	102.5E 58.8S	102.59E 58.67S	-1310	-1900	-1690	-1600	-1625	-2660	1.035
19	Pasteur CC	104.9E 11.8S	105.15E 11.96S	-920	-900	-1010	-1010	-960	-1130	0.170
20	Jules Verne CC		143.76E 37.23S	-1620	-1560	-1550	-1570	-1575	-1920	0.345
21	Jules Verne CC SE	144.1E 37.5S	144.33E 37.40S	-1420	-1530	-1360	-1700	-1502.5	-1760	0.258
22	Geiger CC	159.0E 16.2S	159.01 E 16.11S	110	30	-25	75	47.5	-235	0.283
23	Vertregt K CC	172.6E 20.6S	172.69E 20.50S	-1470	-1780	-1780	-1745	-1693.75	-2100	0.406

Concentric Craters

A small percentage of craters that would normally fall in the classification of simple craters show a curious inner ring (torus or toroid) that averages about 50% of the diameter of the outer ring (Wood, 1978). The crater sizes range from 2-20 km outer diameter with an average outer diameter around 8 km, though most fall within the 2-12 km diameter size. (Note sub-kilometer "bench" craters and multi-ringed basins are not being considered in this paper). They also tend to be shallower in depth than normal craters of similar size which would be expected to have a depth (d) to diameter (D) ratio around 0.2 (Trang et al., 2011).

Concentrics have a non-uniform distribution over the moon that is similar to the distribution floor-fractured craters. Seventy percent of them are found on the margins of maria, 20% in the smooth floors of lava-flooded crater, and 10% in pure highland areas. None are found in the central maria (Wood 1978). Their ages range from Pre-Imbrian (>3.85 Ga) to Eratosthenian (1.1-3.2 Ga), with most of the craters being of Imbrian age (3.2-3.85 Ga). Notably, however, no Copernican age (<1.1 Ga) craters are known to exist on the moon (Trang et al., 2011).

Most, but not all, of the toroid rims are concentric with the outer crater rims and the ratio of the toroid diameter (T) to the outer crater rim diameter (D) range from 0.2 to 0.9 (T/D ratio). Most of the T/D ratios range from 0.3 to 0.6 and average 0.5. While the outer rim margins craters this size are normally slightly concave, the outer margins of the toroid tends to be slightly convex and the area inside the torus is usually concave (Wood, 1979).

While the most notable concentrics have rounded, doughnut-like toroids, others have flattened inner mounds, and a few have sharp inner rims. The space or moat between the inner and outer rims varies in appearance, and a few have confluent lobes of rubble that may give the appearance of another ring between inner and out rings when viewed at low resolution.

Chuck Wood in his 1978 paper describes several variations of morphology. Most common are typified by Hesiodius A with the usual characteristics described above. Marth was described as appearing like a cratered dome. Some craters have elliptical inner and outer rings as typified by the crater in Struve, while others have a round outer ring and elliptical toroid such as Crozier H, which is also off center from outer ring. Craters such as Gruithuisen K have raised, rubbly moat area that resembles a third ring. A few

craters are fractured and cracked, highly worn such as the concentric craters near Mons Jura, and have been described as having "bread crust" appearing interior. Garbart J is shown to have an inner rim that is low and inconspicuous while Chamberlain was described as having a high concentric "collar", but on LROC images looks as if it could possibly be a due to separate impacts.

Various mechanisms have been proposed to explain the formation of the concentric craters. Exogenic hypotheses include a fortuitous double impact either nearly simultaneously by tidally spilt object, a second smaller impact sometime later than the initial impact, or an impact into a layered target. Exogenic origins seem unlikely due to the non-uniform distribution of the craters, due to the presence of non-concentric craters in proximity to concentrics, and also due the lack of Copernican-age concentric craters (Trang, 2010).

Endogenic formation hypotheses include successive eruptions from same vent, symmetrical collapse of the outer rim, or cratering into extrusive domes. Another endogenic hypothesis involves volcanic modification of existing craters by distortion from intrusion of laccoliths below the surface or by extrusion of lava above the surface (Wöhler and Lena, 2009)

Any hypothesis for concentric crater formation must account for the following:

Table 2: Western Hemisphere Diameter Data

	Concentric Craters Study Data								
			LROC	Mean	Geodetic		Geodetic		Mean
		Wood	QuickMap	Crater	Crater Diameter		Toroid Dameter		Toroid
	Crater	Coordinates	Coordinates	Diameter	N-S km	W-E km	N-S km	W-E km	Diameter
24	MacMillan	7.8W 24.1N	7.85W 24.20N	6.8	6.83	6.72	4.10	4.33	4.2
25	Hesiodus A	17.0W 30.1S	17.08W 30.13S	14.4	14.44	14.36	7.13	6.60	6.9
26	Gambart J	18.2W 0.7S	18.21W 0.71S	7.1	7.24	7.04	3.55	4.54	4.0
27	Laplace E CC	21.2W 50.0N	21.25W 50.08N	7.0	6.63	7.37	4.14	4.29	4.2
28	Fontenelle D	23.3W 62.5N	23.43W 62.64N	15.7	15.54	15.90	7.26	7.10	7.2
29	Blancanus C CC	29.1W 66.2S							
30	Marth	29.3W 31.1S	29.35W 31.16S	6.5	6.41	6.64	3.04	3.05	3.0
31	La Condamine F CC	31.3W 57.2N	31.49W 57.35N	5.3	5.38	5.28	1.90	1.90	1.9
32	Hainzel H	33.1W 36.9S	33.16W 36.96S	10.0	9.22	10.73	3.25	4.53	3.9
33	Bouguer B CC	33.8W 53.5N	34.10 W 53.58N	6.6	6.68	6.51	3.24	3.25	3.2
34	Bouguer A CC	34.1W 53.2N	33.81W 53.01N	7.7	8.33	7.09	3.75	3.60	3.7
35	J. Herschel F CC	34.6W 57.7N	34.79W 57.91N	5.9	5.64	6.18	2.07	2.09	2.1
36	Gruithuisen M CC		42.01W 37.15N	4.2	4.12	4.36	2.06	2.07	2.1
37	Gruithuisen CC	41.4W 36.7N	41.55W 36.71N	5.6	5.29	5.90	3.55	3.77	3.7
38	Gruithuisen K	42.7W 35.3N	42.73W 35.38N	6.3	6.53	6.00	1.73	1.60	1.7
39	Clausius E CC	46.8W 35.4S	46.82W 35.40S	8.4	8.71	8.12	4.26	4.09	4.2
40	Mersenius S CC		46.60W, 17.80S	3.7	3.6	3.77	2.42	2.04	2.2
41	Mersenius M	48.3W 21.3S	48.56W 21.34S	5.2	5.25	5.20	2.38	2.70	2.5
42	Louville DA	51.6W 46.6N	51.72W 46.59N	10.7	10.86	10.61	7.67	7.64	7.7
43	Damoiseau BA	59.0W 8.3S	59.11W 8.28S	8.6	8.68	8.58	5.44	5.25	5.3
44	Damoiseau D		63.28W 6.44S	16.9	17.08	16.76	12.04	11.51	11.8
45	Lagrange T CC	62.0W 33.0S	62.37W 32.82S	8.3	8.06	8.50	4.07	4.11	4.1
46	Lagrange T	62.4W 32.9S	62.71W 32.97S	11.6	12.00	11.14	5.37	5.38	5.4
47	Markov CC	64.8W 52.6N	66.35W 52.68N	7.1	6.55	7.67	2.80	2.98	2.9
48	Crüger CC	65.7W 17.0S	65.84W 16.99S	2.3	2.29	2.26	1.31	1.47	1.4
49	Rocca F CC	67.1W 14.2S	67.29W 14.23S	3.2	3.34	2.97	1.29	1.18	1.2
50	Cavalerius E	69.9W 7.7N	70.04W 7.66N	9.2	9.05	9.26	4.00	4.18	4.1
51	Lavoisier A CC	75.0W 36.7N	74.99W 37.38N	2.7	2.77	2.67	1.32	1.34	1.3
52	Repsold A	77.5W 51.9N	76.98W 51.82N	7.8	7.83	7.75	4.97	4.75	4.9
53	Struve CC	77.7W 22.0N	78.87W 21.92N	6.2	6.87	5.53	2.80	2.07	2.4
54	Lavoisier CC	81.1W 38.4N	81.24W 38.34N	5.6	5.92	5.25	3.09	2.71	2.9
55	Minkowski CC	143.0W 56.6S	143.95W 56.31S	12.2	11.57	12.83	7.16	6.32	6.7
56	Apollo CC	154.2W 31.0S	154.06W 30.76S	11.6	11.66	11.47	5.83	5.79	5.8
57	De Vries CC	172.7W 20.6S							

- The non-uniform distribution of the concentric craters
- The lack of Copernican age craters.
- Presence of normal non-concentric craters of younger age in close proximity to some of the concentric craters.
- Presence of ejecta blanket remnants around several of the concentric craters.
- 5. Shallow depth compared to similar non-concentric craters
- Spectroscopic studies showing the interior composition to be very similar to the surrounding terrain.

Of the various hypotheses, volcanic modification of the crater appears to be most likely candidate, and spectral studies support the intrusive model. Trang (2011) describes the process: "The idea suggests that dikes have propagated into impact-induced fractures producing a laccolith. The laccolith grows, uplifting the crater floor. The inner torus is created either because impact melt in the center of the crater is inhibiting uplift or the floor relative to the sides, or inflation is followed by a large deflation or collapse." The process is further described by Wohler and Lena (2011): "At the bottom of the transient cavity, however, the flexural rigidity of the overburden and the overburden weight per unit area were reduced to 30% and 61% of their original values, respectively, according to the relations given in [4,10]. If the impact occurred during the magma intrusion phase, the thinned part of the overburden was probably unable to resist the pressurized magma, which in turn may have lifted up the crater floor, thus leading to the shallow crater depth. In this line of thought, the inner depression of the concentric crater is a remnant of the original bowl-shaped crater floor."

Table 2A: Western Hemisphere Elevation/Depth Data

	Concentric Craters Study Data									
			LROC					Mean Rim	Central	Mean
		Wood	QuickMap	Geodetic Crater Rim Elevation				Elevation	Elevation	Crater
	Crater	Coordinates	Coordinates	North (m)	South (m)	West (m)	East (m)	(meters)	(meters)	Depth (km)
24	MacMillan	7.8W 24.1N	7.85W 24.20N	-1750	-1770	-1710	-1740	-1742.5	-2180	0.438
25	Hesiodus A	17.0W 30.1S	17.08W 30.13S	-1040	-1020	-920	-900	-970	-2320	1.350
26	Gambart J	18.2W 0.7S	18.21W 0.71S	-895	-990	-960	-1070	-978.75	-1280	0.301
27	Laplace E CC	21.2W 50.0N	21.25W 50.08N	-3030	-3020	-2770	-2845	-2916.25	-3070	0.154
28	Fontenelle D	23.3W 62.5N	23.43W 62.64N	-2490	-2350	-2050	-2560	-2362.5	-3130	0.768
29	Blancanus C CC	29.1W 66.2S								
30	Marth	29.3W 31.1S	29.35W 31.16S	-905	-910	-930	-680	-856.25	-1195	0.339
31	La Condamine F CC	31.3W 57.2N	31.49W 57.35N	-2440	-2420	-2400	-2370	-2407.5	-2900	0.493
32	Hainzel H	33.1W 36.9S	33.16W 36.96S	85	390	320	-90	176.25	-520	0.696
33	Bouguer B CC	33.8W 53.5N	34.10 W 53.58N	-2540	-2670	-2540	-2240	-2497.5	-2790	0.293
34	Bouguer A CC	34.1W 53.2N	33.81W 53.01N	-2590	-2390	-2580	-2620	-2545	-2830	0.285
35	J. Herschel F CC	34.6W 57.7N	34.79W 57.91N	-2403	-2357	-2140	-2320	-2305	-2500	0.195
36	Gruithuisen M CC		42.01W 37.15N	-1870	-2070	-1980	-1840	-1940	-2120	0.180
37	Gruithuisen CC	41.4W 36.7N	41.55W 36.71N	-1705	-1730	-1800	-1730	-1741	-2060	0.319
38	Gruithuisen K	42.7W 35.3N	42.73W 35.38N	-1920	-2010	-1950	-1970	-1962.5	-2420	0.458
39	Clausius E CC	46.8W 35.4S	46.82W 35.40S	300	680	420	590	497.5	-200	0.698
40	Mersenius S CC		46.60W, 17.80S	-1830	-1780	-1700	-1790	-1775	-1970	0.195
41	Mersenius M	48.3W 21.3S	48.56W 21.34S	-2120	-2050	-1910	-2110	-1775	-2420	0.645
42	Louville DA	51.6W 46.6N	51.72W 46.59N	-1930	-2020	-1950	-1990	-1972.5	-2580	0.608
43	Damoiseau BA	59.0W 8.3S	59.11W 8.28S	-1400	-1310	-1370	-1410	-1372.5	-1910	0.538
44	Damoiseau D		63.28W 6.44S	0	-250	-100	-300	-162.5	-2800	2.638
45	Lagrange T CC	62.0W 33.0S	62.37W 32.82S	690	-410	300	-150	107.5	-430	0.538
46	Lagrange T	62.4W 32.9S	62.71W 32.97S	150	190	-380	-110	-37.5	-1030	0.993
47	Markov CC	64.8W 52.6N	66.35W 52.68N	-2170	-2030	-2080	-2020	-2075	-2230	0.155
48	Crüger CC	65.7W 17.0S	65.84W 16.99S	-1626	-1629	-1638	-1607	-1625	-1668	0.043
49	Rocca F CC	67.1W 14.2S	67.29W 14.23S	-1586	-1506	-1525	-1530	-1536.75	-1662	0.125
50	Cavalerius E	69.9W 7.7N	70.04W 7.66N	-1120	-1440	-1210	-1640	-1352.5	-2060	0.708
51	Lavoisier A CC	75.0W 36.7N	74.99W 37.38N	-1955	-1980	-2050	-2010	-1998.75	-2195	0.196
52	Repsold A	77.5W 51.9N	76.98W 51.82N	-1580	-1700	-1410	-1460	-1537.5	-2580	1.043
53	Struve CC	77.7W 22.0N	78.87W 21.92N	-1310	-1180	-1240	-1040	-1192.5	-1720	0.528
54	Lavoisier CC	81.1W 38.4N	81.24W 38.34N	-1930	-2060	-2025	-1880	-1973.75	-2340	0.366
55	Minkowski CC	143.0W 56.6S	143.95W 56.31S	-6520	-6370	-6610	-5700	-6300	-7090	0.790
56	Apollo CC	154.2W 31.0S	154.06W 30.76S	-3820	-3800	-3760	-3760	-3785	-5050	1.265
57	De Vries CC	172.7W 20.6S								

Purpose of current study

The current study was undertaken to use LROC data to obtain high resolution images, to determine coordinates of the crater centers, measure the diameters of the outer rim crests (D) and toroid rim crests (T), and the crater depths (d). The toroid/crater diameter (T/D) ratio and the dept (d)/diameter (D) ratios were calculated from the measured data.

Craters studied included the concentrics listed by Chuck Wood in 1978, most of the other craters listed in the http://the-moon.wikispaces.com/Concentric+Crater website (Wood et al., 2007), and a few other concentric craters discovered by internet search. One concentric, Fracastorius E, was accidently "discovered" while measuring another concentric; the "discovered" concentric, as usual, had already been described earlier by Chuck Wood, but was not in his original paper.

Methods

The craters were located on the LROC ACT-REACT QuickMap, the coordinates of the apparent center of the craters recorded and the diameters and depths measured and recorded. The diameter measurements were made by placing the QuickMap cursor over one rim crest and tracing a line (query path) through the center of the crater to the crest of the opposite side of the rim and reading the geodetic distance from the Path Query box. In some cases, where parts of the rim were obliterated in the desired area of measurement, the diameters were measured from northwest to southeast and from northeast to southwest and the averages taken. (Note: Geodetic distance was used since the cartographic distance was subject to cylindrical distortion.) Elevation plots were obtained from query paths drawn across the center of the crater (one from west to east and the other from north to south) that extended well beyond the outer crater rim, and elevation profiles were obtained from the Query Results box. Four rim elevation data points were obtained and two central crater elevation points were obtained. The deepest central crater elevation was subtracted from the mean of the rim elevation to determine the crater depth.

Eastern hemisphere diameter measurements and calculations are listed in Table 1 and elevation measurements and crater depth calculations are presented in Table 1A. Corresponding western hemisphere measurements are listed in Table 2 and Table 2A. Depth/diameter ratio and toroid diameter/crater

Table 3: Eastern Hemisphere Depth/Diameter and Toroid Ratio Calculations

	Concentric Craters Study Data							
			LROC	Crater			Toroid (T)	
		Wood	QuickMap	Depth (km)	Diameter	d/D		
	Crater	Coordinates	Coordinates	(d)	(D)	Ratio	Diameter	T/D Ratio
1	Archytas G	0.4E 55.8N	0.53E 55.74N	0.435	7.0	0.062	4.5	0.63
2	Archytas G-b		0.48E 55.56N	0.304	4.3	0.070	2.2	0.51
3	Reaumur B CC	1.3E 4.5S	1.24E 4.52S	0.261	4.4	0.059	2.8	0.64
4	Egede G	6.8E 51.9N	6.93 E 52.00N	0.560	7.3	0.077	5.3	0.73
5	Pontanus E	13.3E 25.2S	13.25E 25.22S	0.848	12.5	0.068	8.2	0.65
6	Torricelli R CC	26.6E 6.4S	26.64E 6.38S	0.205	3.8	0.054	1.2	0.32
7	Beaumont P CC	29.6E 19.1S	29.63 E 19.14S	0.523	11.7	0.045	5.4	0.46
8	Fracastorius E		31.02 E 20.23S	0.895	11.9	0.075	4.4	0.37
9	Crozier H	49.4E 14.1S	49.38E 14.01S	1.008	10.7	0.094	5.0	0.47
10	Endymion SW CC	50.6E 51.7N	51.06E 51.68N	0.243	6.8	0.036	2.8	0.41
11	Apollonius N	64.0E 4.7N	63.76E 4.74N	1.295	10.5	0.124	5.6	0.53
12	Legendre CC	68.2E 27.5S	68.14E 27.81S	0.244	4.4	0.056	1.6	0.36
13	Dubyago CC	69.0E 3.7N	68.61E 3.67N	0.206	5.9	0.035	2.7	0.46
14	Schubert N CC	74.0E 2.0N	73.61E 1.33N	0.473	10.2	0.046	5.5	0.54
15	Humboldt CC	83.2E 26.5S	83.36E 26.55S	0.905	8.5	0.107	3.9	0.46
16	Hamilton CC	84.7E 44.2S	84.73E 44.39S	0.650	11.6	0.056	5.9	0.51
17	Jeans CC	94.4E 53.1S	94.61E 53.13S	0.885	24.2	0.037	16.2	0.67
18	Chamberlin CC	102.5E 58.8S	102.59E 58.67S	1.035	8.3	0.124	6.3	0.75
19	Pasteur CC	104.9E 11.8S	105.15E 11.96S	0.170	6.4	0.026	3.5	0.55
20	Jules Verne CC		143.76E 37.23S	0.345	5.6	0.062	3.0	0.54
21	Jules Verne CC SE	144.1E 37.5S	144.33E 37.40S	0.258	7.1	0.036	3.7	0.52
22	Geiger CC	159.0E 16.2S	159.01 E 16.11S	0.283	6.5	0.043	2.7	0.41
23	Vertregt K CC	172.6E 20.6S	172.69E 20.50S	0.406	9.2	0.044	5.3	0.58

diameter ratios are listed in Table 3 for the eastern hemisphere and Table 3A for the western hemisphere.

All measurements were entered into Excel spreadsheet and calculations done using the spreadsheet formulas. Once all the data had been assembled and calculations done, each measurement was repeated. Any positional error greater than 0.02 degrees and any diameter error greater than 0.2km was measured a third and fourth time, and corrections were made as needed. The coordinates were also cross-checked with Chuck Wood's measurement and any discrepancies were again measured.

Images were obtained from LROC WMS Image Map set at the highest possible resolution of the orthographic projection, and a final image was assembled from four frames centered on the concentric using Photoshop Elements 6. Some touch up of brightness and contrast was done as well, and then the photo cropped to desired size. In order to cross check the coordinates, all of the craters were located on the Image Map by entering the coordinates from the spreadsheet into the latitude and longitude boxes in the Map Options box. Only one was found to be in error which was exactly one degree, and that was corrected. (See tables 1, 1A, 2, 2A, 3 and 3A.)

Table 3A: Western Hemisphere Depth/Diameter and Toroid Ratio Calculations

	Concentric Craters Study Data							
			LROC	Crater			Toroid (T)	
		Wood	QuickMap	Depth (km)	Diameter	d/D		
	Crater	Coordinates	Coordinates	(d)	(D)	Ratio	Diameter	T/D Ratio
24	MacMillan	7.8W 24.1N	7.85W 24.20N	0.438	6.8	0.065	4.2	0.62
25	Hesiodus A	17.0W 30.1S	17.08W 30.13S	1.350	14.4	0.094	6.9	0.48
26	Gambart J	18.2W 0.7S	18.21W 0.71S	0.301	7.1	0.042	4.0	0.57
27	Laplace E CC	21.2W 50.0N	21.25W 50.08N	0.154	7.0	0.022	4.2	0.60
28	Fontenelle D	23.3W 62.5N	23.43W 62.64N	0.768	15.7	0.049	7.2	0.46
29	Blancanus C CC	29.1W 66.2S						
30	Marth	29.3W 31.1S	29.35W 31.16S	0.339	6.5	0.052	3.0	0.47
31	La Condamine F CC	31.3W 57.2N	31.49W 57.35N	0.493	5.3	0.092	1.9	0.36
32	Hainzel H	33.1W 36.9S	33.16W 36.96S	0.696	10.0	0.070	3.9	0.39
33	Bouguer B CC	33.8W 53.5N	34.10 W 53.58N	0.293	6.6	0.044	3.2	0.49
34	Bouguer A CC	34.1W 53.2N	33.81W 53.01N	0.285	7.7	0.037	3.7	0.48
35	J. Herschel F CC	34.6W 57.7N	34.79W 57.91N	0.195	5.9	0.033	2.1	0.35
36	Gruithuisen M CC		42.01W 37.15N	0.180	4.2	0.042	2.1	0.49
37	Gruithuisen CC	41.4W 36.7N	41.55W 36.71N	0.319	5.6	0.057	3.7	0.65
38	Gruithuisen K	42.7W 35.3N	42.73W 35.38N	0.458	6.3	0.073	1.7	0.27
39	Clausius E CC	46.8W 35.4S	46.82W 35.40S	0.698	8.4	0.083	4.2	0.50
40	Mersenius S CC		46.60W, 17.80S	0.195	3.7	0.053	2.2	0.61
41	Mersenius M	48.3W 21.3S	48.56W 21.34S	0.645	5.2	0.123	2.5	0.49
42	Louville DA	51.6W 46.6N	51.72W 46.59N	0.608	10.7	0.057	7.7	0.71
43	Damoiseau BA	59.0W 8.3S	59.11W 8.28S	0.538	8.6	0.062	5.3	0.62
44	Damoiseau D		63.28W 6.44S	2.638	16.9	0.156	11.8	0.70
45	Lagrange T CC	62.0W 33.0S	62.37W 32.82S	0.538	8.3	0.065	4.1	0.49
46	Lagrange T	62.4W 32.9S	62.71W 32.97S	0.993	11.6	0.086	5.4	0.46
47	Markov CC	64.8W 52.6N	66.35W 52.68N	0.155	7.1	0.022	2.9	0.41
48	Crüger CC	65.7W 17.0S	65.84W 16.99S	0.043	2.3	0.019	1.4	0.61
49	Rocca F CC	67.1W 14.2S	67.29W 14.23S	0.125	3.2	0.040	1.2	0.39
50	Cavalerius E	69.9W 7.7N	70.04W 7.66N	0.708	9.2	0.077	4.1	0.45
51	Lavoisier A CC	75.0W 36.7N	74.99W 37.38N	0.196	2.7	0.072	1.3	0.49
52	Repsold A	77.5W 51.9N	76.98W 51.82N	1.043	7.8	0.134	4.9	0.62
53	Struve CC	77.7W 22.0N	78.87W 21.92N	0.528	6.2	0.085	2.4	0.39
54	Lavoisier CC	81.1W 38.4N	81.24W 38.34N	0.366	5.6	0.066	2.9	0.52
55	Minkowski CC	143.0W 56.6S	143.95W 56.31S	0.790	12.2	0.065	6.7	0.55
56	Apollo CC	154.2W 31.0S	154.06W 30.76S	1.265	11.6	0.109	5.8	0.50
57	De Vries CC	172.7W 20.6S		No rims or torus to measure, just undulating terrain.				

Graph A: Diameter Distribution

D	# Craters
0 - 2 km	0
2-4 km	5
4-6 km	11
6-8 km	16
8-10 km	9
10-12 km	8
12-14 km	2
14-16 km	2
16-18 km	1
>18 km	1
	55

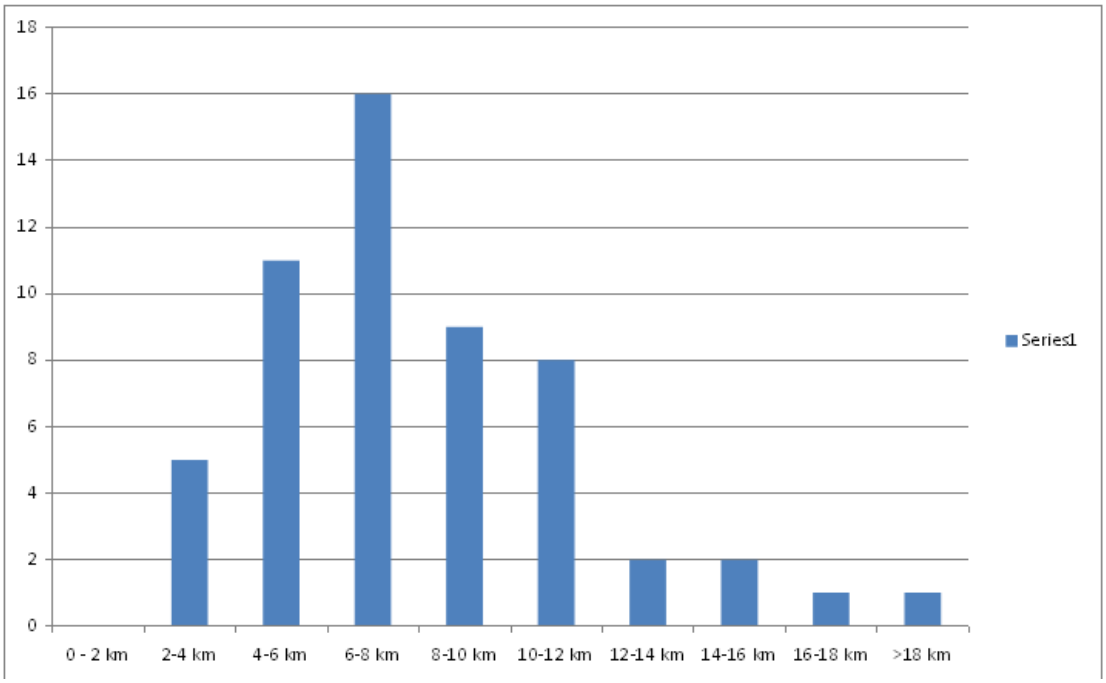

Graph B: Toroid/Diameter Ratios

T/D Ratio	# Craters
<0.2	0
0.2-.03	1
0.3-0.4	8
0.4-0.5	19
0.5-0.6	13
0.6-0.7	11
0.7-0.8	3
>0.8	0
	55

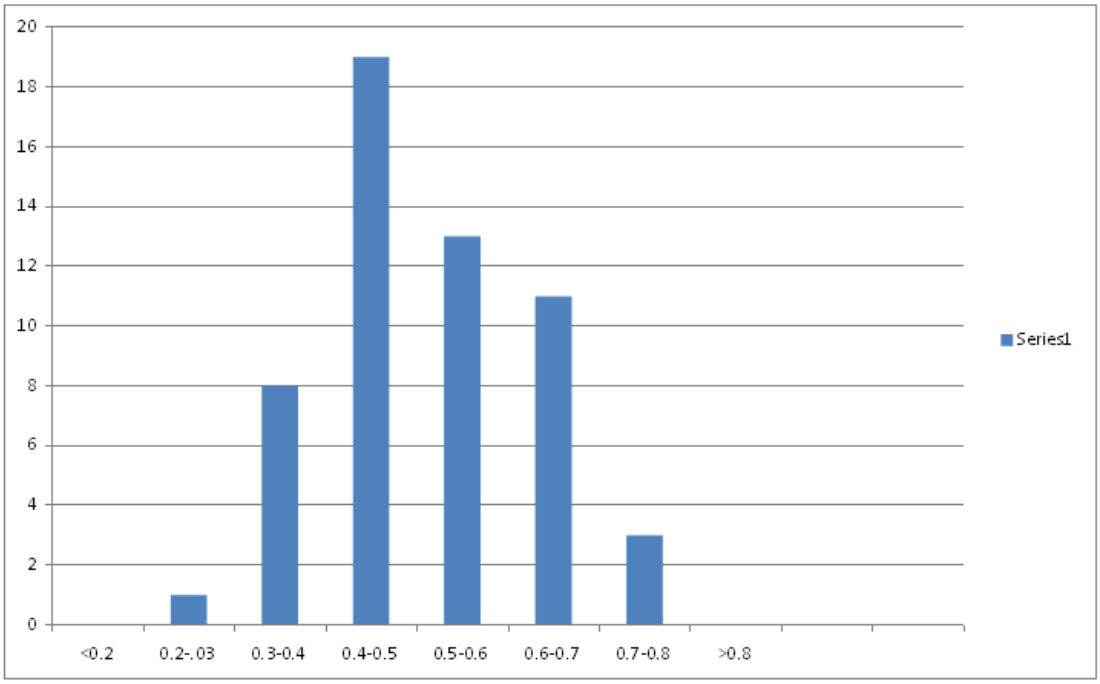

Graph C: Depth/Diameter (d/D) Ratio Distribution

d/D Ratio	# Craters
<0.02	1
0.02-0.04	10
0.04-0.06	16
0.06-0.08	15
0.08-0.10	6
0.10-0.12	2
0.12-0.14	4
>0.14	1
	55

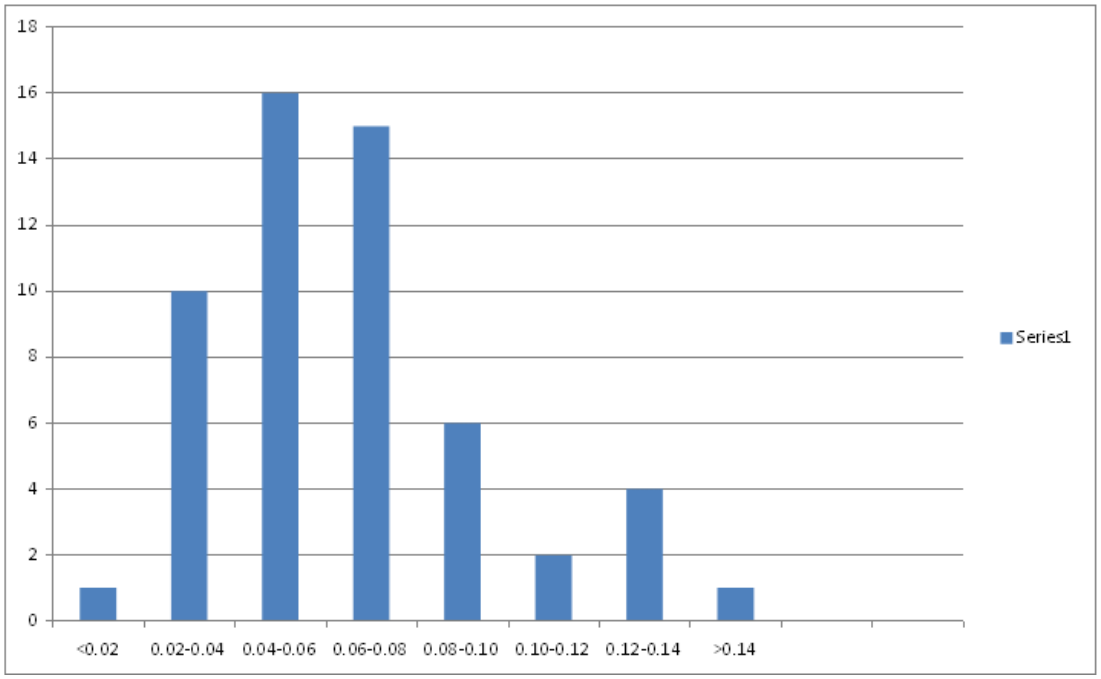

Graph D: Mean Lunar Elevation of Crater Rims

Mean Rim Elevation	# Craters
1 to 0.5km	3
0.5 to 0.0km	5
0.0 to -0.5km	3
-.05 to -1.0km	6
-1.0 to -1.5km	6
-1.5 to -2.0km	18
-2.0 to -2.5km	7
-2.5 to -3.0km	4
-3.0 to -3.5km	1
-3.5k to -4.0km	1
<-4.0km	1
	55

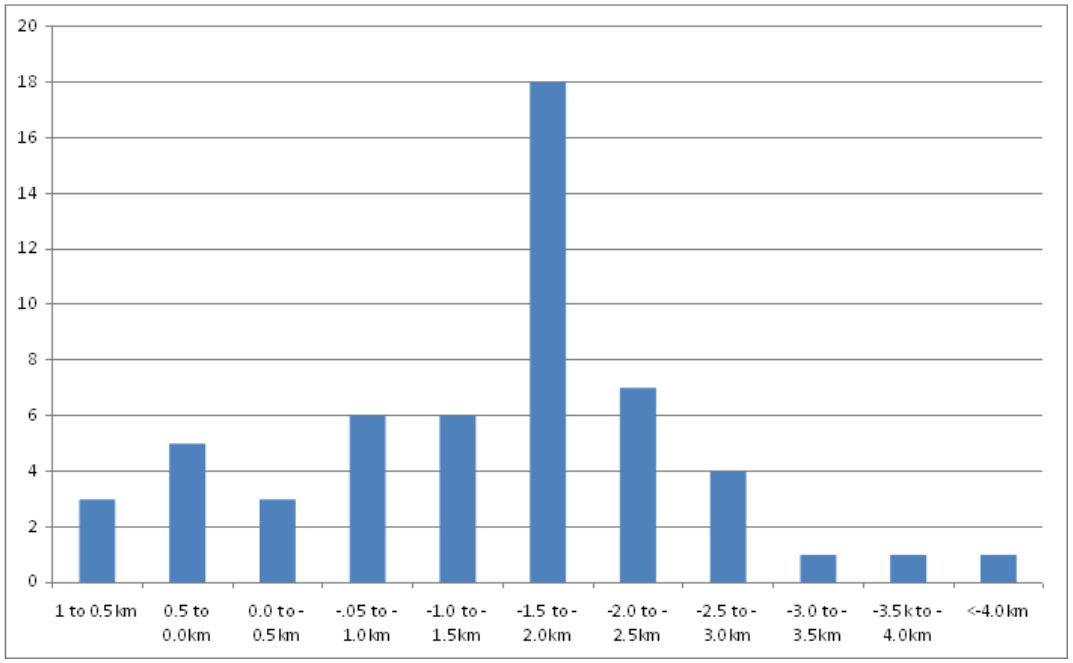

Discussion

Of 57 concentric craters listed on various articles and websites, 55 were measured for rim elevation and diameter, toroid diameter, and depth. Depth/diameter calculations from those data were accurate to two significant figures, and the coordinates for their location were within ±0.02°. Two of the initially listed craters (29 and 57) could not be verified as concentric craters and were excluded from calculations, while seven others (6, 19, 36, 37, 40, 48, and 49) were included in the calculations, but could possibly be something other than a concentric crater.

The 55 craters measured had an average diameter of 8.2 km with nearly half of the craters (27) measuring between 4km and 8km. All of the craters were greater than 2 km diameter, but only 6 craters were greater than 12 km. The largest concentric measured 24.2km; this skewed the mean to the right. (See Graph A.)

The mean toroid diameter was 4.3km and the mean toroid/diameter (T/D) ratio was 0.51. All were between 0.2 and 0.8; only one crater had a ratio smaller than 0.3, and three craters had T/D ratios greater than 0.7. (See Graph B.)

Depth/Diameter (d/D) ratios were considerably shallower than would be expected from a typical crater of the same size as the concentric craters. Normally a d/D ratio of 0.2 would be expected, but the mean d/D of the concentrics measured was 0.065 with only seven craters with a d/D ratio greater than 0.10. The deepest concentric crater had a d/D of 0.156. (See Graph C.)

Thirty-seven of the 55 craters measured had rim elevations between 0.5km and 2.5km below the lunar mean radius of 1737.4 km (per LROC ACT REACT QuickMap), with a distribution peak in the -1.5 to -2.0 km elevation range. The highest mean crater rim elevation was 0.627km above the mean lunar radius (Crozier H) while the lowest rim elevation was recorded in the South Pole-Aitkins Basin at a depth of -6.3 km (near Minkowski). The elevation distribution is consistent with the distribution of the majority of the craters along the margins of maria which are mostly on the near side of the moon. (See Graph D.)

Conclusion

Images of concentric craters from the LROC WMS Map and measurements from the LROC ACT-REACT QuickMap were used to measure crater coordinates, crater rim (D) and toroid (T) diameters, and T/D rations crater rim elevation and crater depths (d) were measured, and used to calculate d/D ratios of each of the selected concentric craters using the latest data available from the Lunar Reconnaissance Orbiter.

The mean rim diameter of 8.2 km is within limits of error of Wood's (1978) mean of 8.3km, while the mean T/D ratio of 4.3 is slightly lower his ratio ~0.5. Several of the concentrics had indistinct and irregular toroid margins that added uncertainty to their measurements.

Measurements of crater rim elevations and depth allowed the d/D ratios to be calculated to two significant figures. The mean d/D was 0.065 which is considerably shallower than the d/D ratio of ~0.2 for ordinary craters of similar size. This suggests that modification of the interiors of the craters occurred after formation and is consistent with the currently favored hypothesis of igneous intrusion for the origin of concentric craters. However, it is possible that not all of the concentric craters formed in that manner. For example, the concentric crater near Chamberlin looks very much like a fortuitous second smaller impact within an older crater.

There is much more to be learned about these fascinating craters by more detailed study of each individual crater and their context to further characterize their morphologies and from spectral analysis of their interiors and surroundings.

References

Albers, S., 2005. Jens Meyer Moon Map, URL: *http://www.lpod.org/?m=20060827 http://laps.noaa.gov/albers/sos/sos.html* (last date accessed: 11 July 2013).

Eskildsen, H., Lena, R., 2011. *Humboldt: Concentric Crater and LPDs*. Selenology Today 25, pp. 1-16.

Eskildsen, Howard, 2013. Archytas G Concentric Crater. Selenology Today 31, pp. 25-28. URL: *http://www.lunar-captures.com//Selenologists/selenologytoday31.pdf*

Trang, D., 2010. *The Origin of Lunar Concentric Craters.* 2010 GSA Denver Annual Meeting.

Trang, D., Gillis-Davis J., Hawke, B., Bussey, D., 2011. *The Origin of Lunar Concentric Craters.* 42nd Lunar and Planetary Science Conference.

Wöhler, C and Lena, R., 2009. The Lunar Concentric Crater Archytas G Associated with an Intrusive Dome. Lunar and Planetary Science Conference XXXX. Abstract1091, The Woodlands, Texas. URL: *http://www.lpi.usra.edu/meetings/lpsc2009/pdf/1091.pdf*

Wood, C.A., 1978. *Lunar Concentric Craters.* Lunar and Planetary Science Conference IX, pp.1,264-1,266.

Wood, C., 2004. Concentric Craters LPOD June 23, 2004, URL: *http://www.lpod.org/archive/archive/2004/06/LPOD-2004-06-23.htm* (last date accessed: 11 July 2013).

Wood, C., 2006. Concentric Craters, URL: *http://www.lpod.org/?m=20060827* (last date accessed: 11 July 2013).

Wood, C., Caes, D., Mosher, J., Moore, J., 2007. Concentric Craters, URL: *http://the-moon.wikispaces.com/Concentric+Crater*, (last date accessed: 11 July 2013).